Wiley Online Library
Early View publication on www.wileyonlinelibrary.com
(issue and page numbers not yet assigned;
citable using Digital Object Identifier – DOI)

Phys. Status Solidi C, 1–5 (2015) / DOI 10.1002/pssc.201400230

physica status solidi c
www.pss-c.com
current topics in solid state physics

Control of extended defects in cast and seed cast Si ingots for photovoltaic application

Takashi Sekiguchi[*,1,2], Karolin Jiptner[1], Ronit R. Prakash[1,2], Jun Chen[1], Yoshiji Miyamura[1], Hirofumi Harada[1], S. Nakano[3], Bin Gao[3], and Koichi Kakimoto[3]

[1] MANA Nanoelectronic Materials Unit, National Institute for Materials Science, Tsukuba 305-0044, Japan
[2] Doctoral Program for Pure and Applied Sciences, University of Tsukuba, Tsukuba 305-0044, Japan
[3] Research Institute for Applied Mechanics, Kyushu University, Fukuoka 816-8580, Japan

Received 12 September 2014, revised 1 May 2015, accepted 18 May 2015
Published online 11 June 2015

Keywords Si, cast growth, seed cast, grain boundary, dislocation

* Corresponding author: e-mail Sekiguchi.takashi@nims.go.jp, Phone: +81 29 860 4297, Fax: +81 29 860 4794

We discuss the defect evolution in conventional cast and seed cast Si ingot growths for photovoltaic application. Three different cast Si ingots were grown in one directional solidification furnace. The two extremes are the seed cast ingots (mono-Si), where growth starts from monocrystalline silicon seeds, and the multicrystalline silicon grown from small randomly oriented grains. The conventional multicrystalline (mc-) cast Si ingots are grown without any seeds and have grain structures in between the two extremes. It was found that in mc-Si the evolution of grain boundaries take place in several steps. On the other hand, the major defects in mono-Si are dislocations and are generated by stress due to thermal gradient in the ingot.

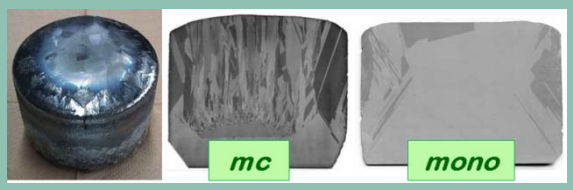

Photograph of 10 cm diameter Si ingot and the cross section of mc- and mono Si.

1 Introduction Cast growth technique is the most widely used method to produce multicrystalline (mc-) Si for photovoltaic application. The solar cells made from such cast grown mc-Si wafers generally yield about 2 % lower efficiency than those made from monocrystalline Si wafers. To improve the efficiency of cast Si ingots, many attempts have been proposed and demonstrated so far [1-5]. Among them, the most ambitious attempt is the seed cast growth method, which was proposed by the BP Solar group [4,5]. Although many institutes are involved in this method now, it may take more time to put it to mass production [6-8].

To improve the efficiency of cast Si solar cells, the reduction of extended defects, metallic impurities and light element impurities are the three main issues. In this paper we will mainly focus on the control and reduction of extended defects.

Cast ingots of 10 cm diameter were grown using a pilot furnace (Toyota Technological Institute; TTI). Some mc-Si ingots were grown by the conventional method (without seeds) while others were grown from microcrystalline Si templates which have small and randomly oriented grains. Mono Si ingots were grown on CZ-Si seed crystals. The generation and propagation of extended defects in both mc- and mono-Si ingots are discussed in this paper.

2 Experimental 10 cm diameter mono cast Si ingots were grown using an unidirectional growth furnace as shown in Fig. 1(a) [9,10]. Si seed crystal of (001) orientation and Si feedstock with a weight of about 2 kg was charged in quartz crucible coated with Si_3N_4 powder. The feedstock was heated above 1500 ºC and kept for 1 h. Then the crucible was moderately pulled down and the heater power was reduced for solidification. Thus, the solidification starts from the bottom of the melt to the top. The typical temperature history and heater position are shown in Fig. 1(b). Ar gas of 1 to 2 slm was passed into the furnace

during the crystal growth. To reduce carbon contamination, the materials of the gas tube and the cover on the crucible were considered. After the growth, the center of the ingots was sliced vertically with 1 or 2 mm thickness and its surface was chemically polished for further evaluation.

More than 30 ingots were grown by changing the growth condition systematically. For the seed cast, the growth conditions were set to prevent complete melting of the seed. Similarly to realize growth from small randomly oriented grains, the feedstock (high purity microcrystalline silicon) was used as the seed, hence not melted completely.

The quality of ingots was characterized by various methods using the vertically cut slices. First, the grain structure was imaged by optical micrographs and the grain boundary characters were determined using electron backscattered diffraction (EBSD) method. Fourier Transform Infrared Spectrometer (FTIR) was used to measure C, O, N concentrations. Scanning infrared polariscope (SIRP) was used to evaluate the distribution of residual strain. X-ray topography (XRT) was used for imaging the extended defects. Electron beam induced current (EBIC) was used to observe the electrically active defects.

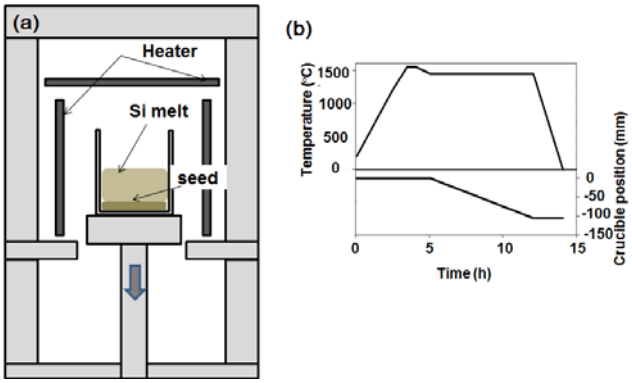

Figure 1 (a) Unidirectional growth furnace and (b) growth condition.

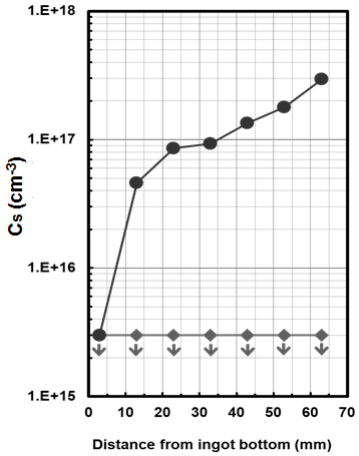

Figure 2 Variation of substitutional carbon (Cs) concentrations (●) before and (◆) after development.

3 Results and discussion

To supress the other avoidable factors which give multicrystallization or degrade the crystal quality, the carbon and nitrogen incorporation has been minimized. Carbon incorporation was suppressed by controlling the Ar gas flow. Figure 2 shows the C concentration at different heights of the ingot before (●) and after (◆) improvement. Nitrogen incorporation was also reduced by improving the coating procedure of crucible. After these developments, multicrystallization due to SiC or Si_3N_4 particles has been significantly reduced.

The appearance of ingots and their vertical cuts are shown in Fig. 3. Figure 3(a) shows the conventionally grown mc-Si (without seed), (b) shows mc-Si grown from the feedstock, (c) is the monocrystal Si grown from seed crystal, although twin boundaries have been introduced from the sidewall, most of the ingot is monocrystalline.

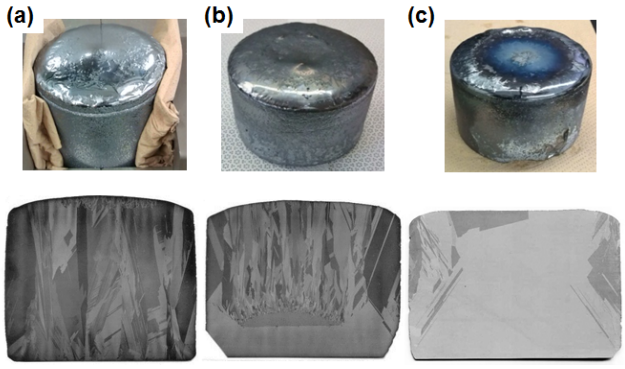

Figure 3 Photographs of ϕ10 cm ingot faces and vertical cuts, (a) mc, (b) mc grown from feedstock, (c) mono (seeded).

3.1 mc-Si ingots It is rather difficult to classify the quality of mc-Si ingots. The grain size, grain orientation, and the grain boundary (GB) characters are different due to the growth conditions of different furnaces. However, under the same condition, the statistics of these characteristics become similar. In our mc-ingots without any seeds, the grain size at the initial stage becomes as large as several mm. Further growth does not seem to introduce significant change of grain structure. For the study of grain reaction during the growth, the ingots grown from the feedstock are suitable. As shown in Fig. 3(b), the grains start to grow on the microcrystalline template with random orientation. The grains become larger as solidification proceeds. This behaviour has been discussed in Ref. [11].

Figure 4 shows the magnified image of vertically cut mc-Si ingot grown on feedstock. The EBSD image shows the existence of twin boundaries as well as the variation of grain orientation. It is clearly seen that small grains appear at the beginning of crystal growth and they quickly become large to a certain size, then the grains become elongated to the growth direction. Finally, the columnar structure appears.

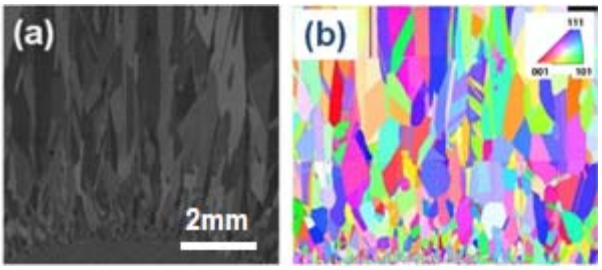

Figure 4 Vertical cut of mc-Si ingot grown on feedstock. (a) Optical image, (b) EBSD mapping of grain structure.

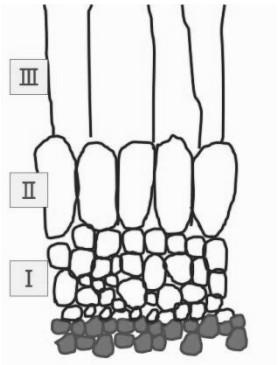

Figure 5 A model of grain evolution.

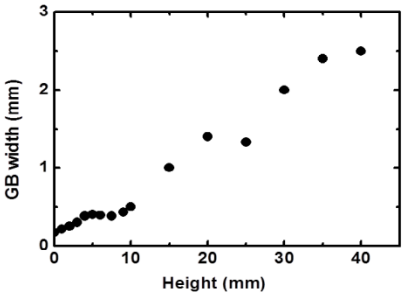

Figure 6 Variation of average grain width along growth height.

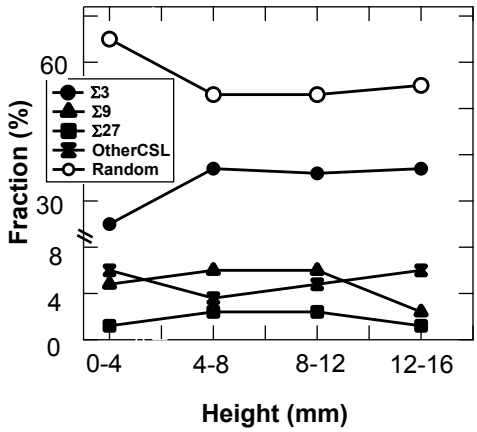

Figure 7 Variation of GB character along growth height.

Such variation is shown in Fig. 5. Namely, the grains become larger in 3 stages. According to the grain evolution, the shape of grains changes from spherical (I), ellipsoidal (II) to columnar (III). The average width of grains was measured according to the growth height and is shown in Fig. 6. The variation is not straight, which indicates that the grain evolution takes place according to several factors.

To clarify this reaction, the grain boundary character was observed by EBSD technique. Figure 7 shows the fractional variation of GB character along the growth height. When the height reaches to 16 mm, the fraction does not change significantly. (Due to the small number of grain boundaries the data are not plotted.) Most of the GBs in this ingot are Σ3 or random. Minorities are Σ9 and Σ27. At the initial stage of crystal growth, random GB has the highest fraction with 65 %, while Σ3 is 25 %. According to the growth, random GB fraction becomes smaller and Σ3 larger. Such fractional change has ended around 4-8 mm height. This suggests that the GB reaction has mainly taken place at the initial stage of crystal growth. This behaviour is somewhat different from that of conventionally grown mc-Si without any template. The randomly oriented microcrystalline template may be the reason of this reaction. The detailed study is now on the way.

The above observation suggests that we may control the grain structure of mc-Si by using some special templates. Recent report of high performance multi crystalline (HP-mc) Si may indirectly utilize this idea.

3.2 mono-Si ingots Mono-Si growth by seed cast method is the core purpose of this study. The high quality and low cost mono-Si wafer may reduce the wattage cost of Si solar cells. Although the laboratory size ingots are not so difficult to grow, we have to overcome several difficulties to produce mass production size ones. This effort is going on with 50 cm square ingot furnace [8]. Another aspect is improvement of mono-Si quality. Besides transition metal and light element impurities, the mono-Si includes structural defects like dislocations or lineages (bundle of dislocations). It is known that dislocation related defects suppress the lifetime. Arafune et al. found that minority carrier lifetime decreases as the etch pit density increases in mc-Si. [12] Thus, reduction of such defects is important to obtain high-quality mono-Si. The mono Si ingot may also be accompanied with residual strain. It should be smaller to avoid wafer fracture during process.

As shown in Fig. 3(c), our mono crystals are not perfect as the twin boundaries are frequently introduced from the bottom edge. These twins, however, do not affect the electrical or mechanical properties so much. Figure 8 shows X-ray topographs of vertically cut wafers from the ingots grown at the early stage of this project. Ingot #8 (a) has several dark bands from bottom to top. They are lineages, namely bundle of dislocations. Improving the condition of onset of the growth, the lineages are almost suppressed as in ingot #10 (b), which only has a weak line at

the center as well as several at the periphery. Reduction of lineages and other grown-in defects are possible to a certain level by growth improvement.

The lineage suppressed ingots were then supplied for the residual strain measurement. Figure 9 shows the SIRP images of ingots that were slowly cooled or fast cooled after solidification. It is clearly seen that the fast cooled one contains much higher residual strain than the slowly cooled one. In both cases, the outer region has higher strain than the inner part. This strain is mainly elastic and is reduced if the vertical wafers are cut in pieces. However, at high temperatures, this strain acts as the driving force of dislocation generation and multiplication. The lineages and other defective parts are also seen as higher strain areas.

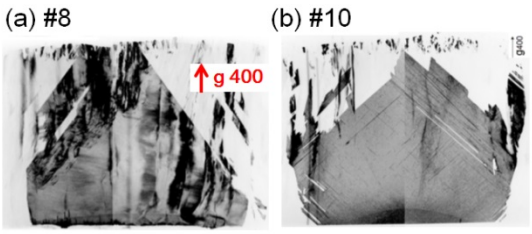

Figure 8 XRT images of (a) bad and (b) better mono-Si.

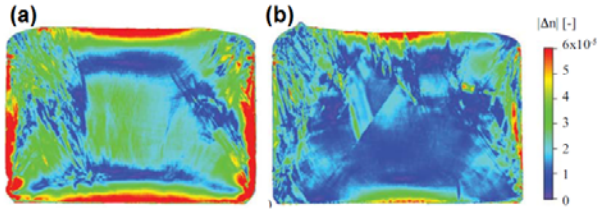

Figure 9 SIRP images of (a) slowly and (b) fast cooled ingot.

The relation between residual strain and dislocation distribution is rather difficult to analyze. It is because the ingot has experienced its thermal history after solidification and it suffers deformation by the stress due to the thermal gradient in the ingot as well as the due to the constraint of thermal expansion difference. The latter may be significantly reduced if the coating has been done properly. The thermal gradient is inevitable and it increases in the case of fast cooling. This difference of thermal gradient in the ingot may give the significant difference of residual strain and dislocation density.

The dislocation generation and motion is explained using Haasen-Alexander-Sumino model [13, 14].

$$N_m = Kk_0 \left(\tau_{eff}\right)^{p+\lambda} \exp\left(-\frac{Q}{kT}\right) N_m,$$

where N_m is number of mobile dislocations, τ_{eff} is effective stress, Q is the Peierls potential, T is the absolute temperature, k_0 is the Boltzmann constant, K, p, λ are the material constants. Since Q is 2.2 eV for the double kink formation, the dislocation generation is dominant at higher temperatures. According to this idea, Nakano et al. [15] has simulated the residual strain and dislocation distribution by calculating the temperature distribution during the growth and after the solidification. Their analysis suggests that the dislocation generation is dominant at the tempratures higher than 1200 ºC. According to the temperature decrease, the dislocation cannot be generated and the rearrangement of dislocation reduces the strain. As further cooling below 700 ºC, dislocation become immobile and the residual strain increases. The last dislocation arrangement may yield another strain distribution.

Jiptner et al. [16] have studied how the cooling process is important to reduce the residual strain. They have grown two identical mono ingots and cooled them in different speed below 900 ºC. The slowly cooled ingot (5 ºC/min) in Fig. 9(b) has about 55% lower residual strain than fast cooled one (12 ºC/min) in Fig. 9(a). This is rather consistent with the simulation. On the other hand, the discussion of dislocation densities is rather difficult to compare. The Secco etching experiment showed that the dislocation density is in the order of 10^4 cm^{-2}, which is more than 100 times higher than that of the simulation. This suggests that the density of grown-in dislocation is rather high and they may suppress the quality of mono-Si ingots.

One attempt has been made to estimate the lowest dislocation density in mono Si crystal [17]. For this purpose, a FZ Si ingot of slightly smaller diameter than crucible interior was set into the growth furnace and was subjected to similar thermal history after solidification. Since the FZ Si ingot is dislocation free, we may estimate the effect of dislocation generation during cooling. Figure 10 shows the XRT image of vertical cut wafer of this FZ Si. The characteristic dislocation distribution, namely "X" shape, is consistent with the simulation [18]. The average dislocation density is in the order of 10^3 cm^{-2}, which was also confirmed by Secco etching. It is said that solar cell efficiency may be suppressed when the dislocation density exceeds 10^4 cm^{-2}. Thus, the improved mono Si ingot will be available for the Si wafers of next generation solar cells.

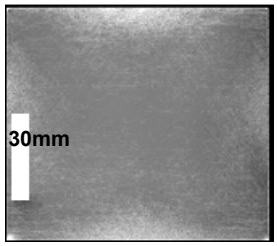

Figure 10 XRT image of thermally treated FZ-Si ingot.

4 Summary The defect evolution in conventional mc-Si, mc-Si grown from microcrystalline template and mono-Si was discussed. The grain evolution and grain boundary reaction was elucidated. For seeded mono-Si growth, strain appears due to thermal gradient in the ingot.

This strain generated dislocations at higher temperatures. Generation of dislocations may partly relax the strain. Such mechanism results in the final residual strain and dislocation distribution in mono-Si ingots.

Acknowledgements This work was partly supported by the New Energy and Industrial Technology Development Organization (NEDO) under the Ministry of Economy, Trade and Industry (METI).

References

[1] S. Nara and T. Sekiguchi, J. Chen, Eur. Phys. J. Appl. Phys. **27,** 389 (2004).
[2] K. Fujiwara, W. Pan, N. Usami, K. Sawada, M. Tokairin, Y. Nose, A. Nomura, T. Shishido, and K. Nakajima, Acta Mater. **54,** 3191 (2006).
[3] T. Y. Wang, S. I. Hsu, C. C. Fei, K. M. Yei, W. C. Hsu, and C. W. Lan, J. Cryst. Growth **311,** 263 (2009).
[4] N. Stoddard, B. Wu, I. Witting, M. Wagner, Y. Park, G. Rozgonyi, and R. Clark, Solid State Phenom. **131–133**, 1 (2008).
[5] B. Wu, N. Stoddard, R. Ma, and R. Clark, J. Cryst. Growth **310,** 2178 (2008).
[6] A. Jouini, D. Ponthenier, H. Lignier, N. Enjabelt, B. Marie, B. Drevet, E. Pihan, C. Cayron, T. Lafford, and D. Camel, Prog. Photovolt.: Res. Appl. **20**, 735 (2012).
[7] M. Trempa, C. Reimann, J. Friedrich, G. Muller, and D. Oriwol, J. Cryst. Growth **351,** 131 (2012).
[8] Y. Miyamura, H. Harada, K. Jiptner, J. Chen, R. R. Prakash, S. Nakano, B.Gao, K. Kakimoto, and T.Sekiguchi, J. Cryst. Growth **401,** 133 (2014).
[9] K. Arafune, E. Oishi, H. Sai, Y. Ohshita, and M. Yamaguchi, J. Cryst. Growth **308,** 5 (2008).
[10] Y. Miyamura, H. Harada, K. Jiptner, J. Chen, R. R. Prakash, J. Y. Li, T. Sekiguchi, T. Kojima, Y. Oshita, A. Ogura, M. Fukuzawa, S. Nakano, B. Gao, and K. Kakimoto, Solid State Phenom. **205-206,** 89 (2014).
[11] R. R. Prakash, T. Sekiguchi, K. Jiptner, Y. Miyamura, J. Chen, H. Harada, and K. Kakimoto, J. Cryst. Growth **401,** 717 (2014).
[12] K. Arafune, T. Sasaki, F. Wakabayashi, Y. Terada, Y. Ohshita, and M. Yamaguchi, Physica B **376-377,** 236 (2006).
[13] H. Alexander and P. Haasen, Solid State Phys. **22,** 27 (1968).
[14] M. Suezwa, K. Sumino, and I. Yonenaga, J. Appl. Phys. **51,** 217 (1979).
[15] K. Jiptner, M. Fukuzawa, Y. Miyamura, H. Harada, K. Kakimoto, and T. Sekiguchi, Phys. Status Solidi C **10,** 141 (2013).
[16] K. Jiptner, M. Fukuzawa, Y. Miyamura, H. Harada, K. Kakimoto, and T. Sekiguchi, Jpn. J. Appl. Phys. **52,** 065501 (2013).
[17] K. Jiptner, B. Gao, H. Harada, Y. Miyamura, M. Fukuzawa K. Kakimoto, and T. Sekiguchi, J. Cryst. Growth **408,** 19 (2014).
[18] B. Gao, K. Jipner, S. Nakano, H. Harada, Y. Miyamura, T. Sekiguchi, and K. Kakimoto, J. Cryst. Growth **411,** 49 (2015).